TAO, Vol.7, No.2, 167-178, June 1996

Source Effects on the Amplitude Variation of Rayleigh Waves From Finite Element Simulations

YEONG TEIN YEH[1,2] and JEN-KUANG CHUNG[3]

(Manuscript received 13 February 1995, in final form 21 March 1996)

ABSTRACT

The two-dimensional finite element method is employed to simulate Rayleigh waves in this study. Various dislocation sources located at various depths are considered. Through the analysis of amplitude variations, the relationships between the excitations of the Rayleigh waves and the faultings are gradually understood. In order to determine the effects due to the damping factor involved in the calculations from the attenuation curves, a simple technique is proposed and applied in this paper. The results show that the amplitude is suppressed to a lower extent with lower frequency signals. In general, Rayleigh-wave excitation from any type of faulting decreases with source depth. The steeper finite faultings at the shallower depth generate stronger Rayleigh waves. For 45° dip-slip sources, it is also easier to generate stronger Rayleigh waves for point sources than for finite ones.

(Key words: Finite element, Rayleigh wave excitation, Source)

1. INTRODUCTION

Short-period surface waves recorded at similar distances and with similar site conditions can vary significantly due to the variability of the source. Hanks (1975) noted that seismic moment, source dimension, radiation pattern and rupture propagation are the most important factors in forming the amplitude and frequency content of strong motion waveforms. Basically, at present there are two regular ways to investigate source effects. First, from the observation point of view, additional near-source data collection should be the most fundamental and crucial task for the inversion of the source parameters (Gariel *et al.*, 1990; Mendez and Anderson, 1991), thereby relating the faulting process with tectonics and seismicity patterns. The other approach involves forward modelings of source geometry and rupture history utilizing numerical techniques because of the great advances with computer facilities

[1] Institute of Seismology, National Chung Cheng University, Chiayi, Taiwan, R.O.C.

[2] Institute of Earth Sciences, Academia Sinica, P. O. Box 1-55, Nankang, Taipei, Taiwan, R.O.C.

[3] Seismology Center, Central Weather Bureau, 64 Kung-Yuan Road, Taipei, Taiwan, R.O.C.

in recent years. The latter seems to be easier and more flexible than the pure theoretical methods, especially with modelings of complex structures and source mechanisms.

For long period surface waves, strong dependence on the source parameters of amplitude excitation was proposed in positive terms by Tsai and Aki (1971). For the intermediate period range, Panza *et al.* (1972) described the displacement versus depth relationships of channel and crustal Rayleigh waves in the presence of a low-velocity channel. They also investigated the characteristics of the Rayleigh waves due to dip-slip motion on a vertical fault plane located at various depths in the crust (Panza *et al.*, 1973). However, the problems for a shorter period still haven't been addressed. The purpose of this study is, therefore, to understand whether the same characteristics observed in the long period can be extended to short period cases. In near-distance simulations, it has been proven that various sources generate identified surface waves at different distances for the elastic half-space and a single layered half-space models, respectively (Yeh and Chung, 1993). In this study, the amplitude intensity on the respective critical epicentral distance of Rayleigh wave initialization for the different types of source parameters are examined.

To make use of the short-period surface wave information from near-distance earthquakes, it is probably necessary to simulate ground motions directly in the time domain. Accordingly, the finite element method is used here. The justification for this is the powerful ability to model complex structures and of the implementation on simulating the rupture sources to the model (Melosh and Raefsky, 1981).

2. METHOD

In view of path length requirements to generate surface waves, the model is designed with a length of 150 km and a width of 50 km, and this prevents the higher-order unwanted reflections that the employed absorbing boundary skill proposed by Smith (1974) cannot eliminate. The signals with the period range of 1 to 3 sec, depending on the element size (1 km square used herein), along with the elastic wave velocities, therefore, can be resolved from the matrix differential full-wave equation:

$$[M]\{\ddot{u}\} + [C]\{\dot{u}\} + [K]\{u\} = \{f\}, \tag{1}$$

where $[M], [C]$ and $[K]$ are the element mass, damping and stiffness matrix, respectively. $\{f\}$, the force vector acting on the nodes, must be replaced by introducing fictitious forces on both the nodes adjacent to the split node and on the split node itself so as to model the discontinuous displacements along the fault (Melosh and Raefsky, 1981). The shape of the slip displacement function $S(t)$ at any point on the fault is defined as a Gaussian function

$$S(t) = e^{-\alpha(t-t_o)^2}, \tag{2}$$

where α is the factor controlling the shape of the amplitude decay from the peak which appears at the time t_o. In this study, the decay factor α of 50 is uniformly set on each of the nodes along the fault, and signals with a dominant period of 0.6 sec are originated from the source.

One of the limitations related to the finite element calculation is the well-known ringing phenomenon due to impulse source excitation (e.g. Shipley *et al.*, 1967). Smith (1975) showed that if the length of the square pulse is chosen as the reciprocal of the ringing

frequency, the ringing can be markedly reduced. However, this criterion basically constrains the flexibility of the source duration. Another approach to reduce the ringing is to apply the damping matrix, $[C]$, which, in practice, generally attenuates the higher frequency ringing. This manner, however, still has inherent shortcomings since the damping employment also attenuates the signals of the interesting frequency band. In light of these drawbacks, the damping effect on the synthetic seismic signals must be taken into account when analyzing the problems concerning amplitude variation. In the following, the authors propose an alternative way to remove the effects of the damping factor on the amplitude.

To simplify the calculations, the damping coefficient, as defined by Archuleta and Frazier (1978), instead of a huge matrix, is usually taken as a constant value in the range of 0.1 to 0.2 set on every element (e.g., Huang and Yeh, 1991). At first, a full-space homogeneous finite element model is constructed with a 45° dip-slip point dislocation source located at the center of the mesh. The P-wave and S-wave velocity are 6.0 and 3.4 km/sec, respectively, while the density is 2.6 gm/cm^3. The source time function described above is used. The displacement waveforms are calculated at different distances along two orthogonal directions (line AA′ and BB′ shown in Figure 1), where the strongest P-waves appear according to the theoretical radiation patterns of amplitude in the far field (Aki and Richards, 1980).

In the time domain, the comparisons of the synthetic seismograms simulated with various damping coefficients can clearly show the damping effect. Figure 2 illustrates some of the traces along line AA′. It can be seen that the main pulses, i.e., P-phases in the vertical component and weak S-phases in the horizontal component, are generally followed by significant ringings when a smaller damping coefficient is involved. The ability to suppress the ringings, in fact, seems to be better at greater distances. Similar results (not shown) are also obtained in the case of the other two directions CC′ and DD′, as indicated in Figure 1, where the S waves are dominant.

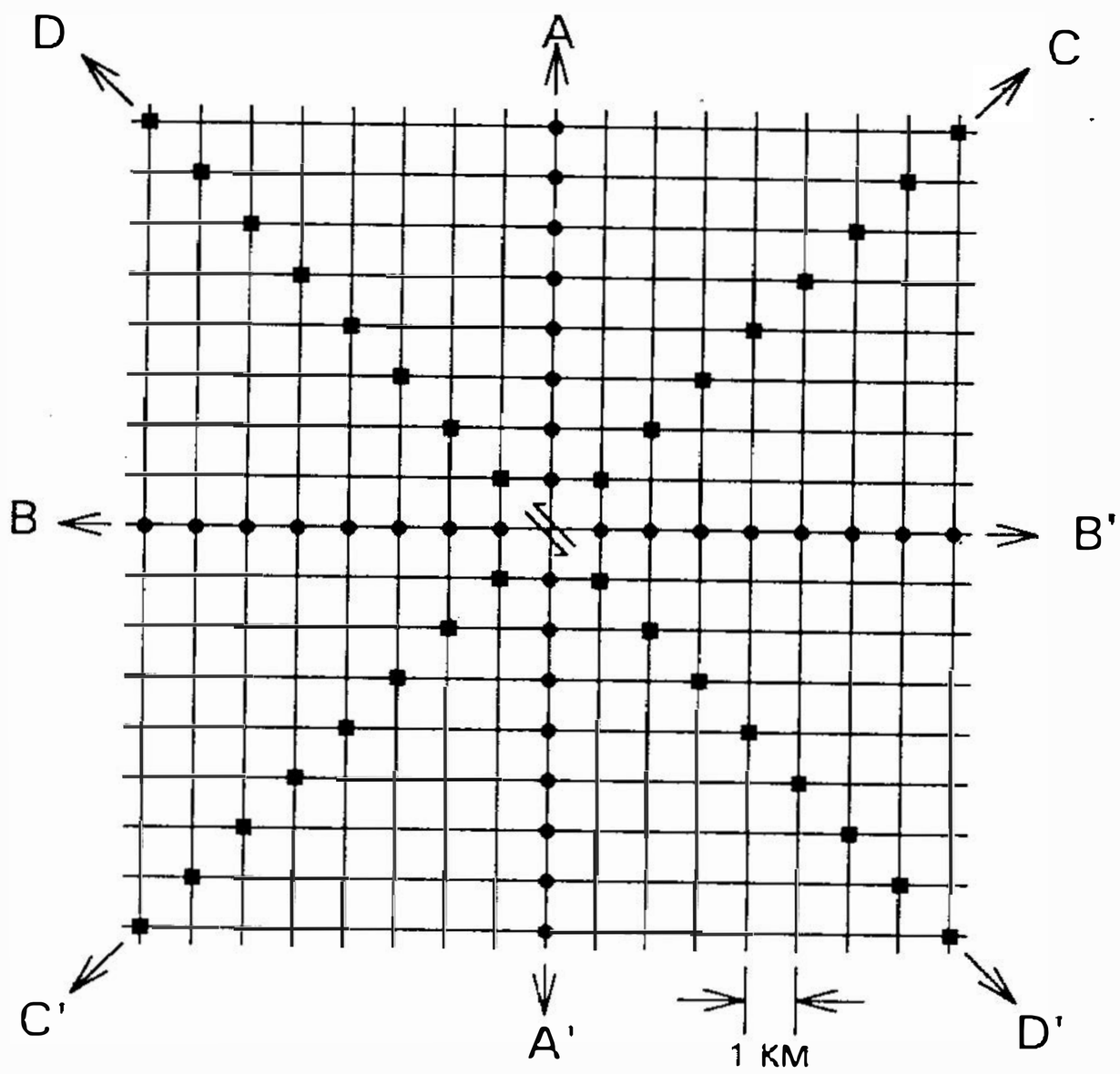

Fig. 1. The full-space model used to simulate seismograms along the lines AA′, BB′, CC′ and DD′ for a 45° dip-slip point dislocation source located at the center of the model.

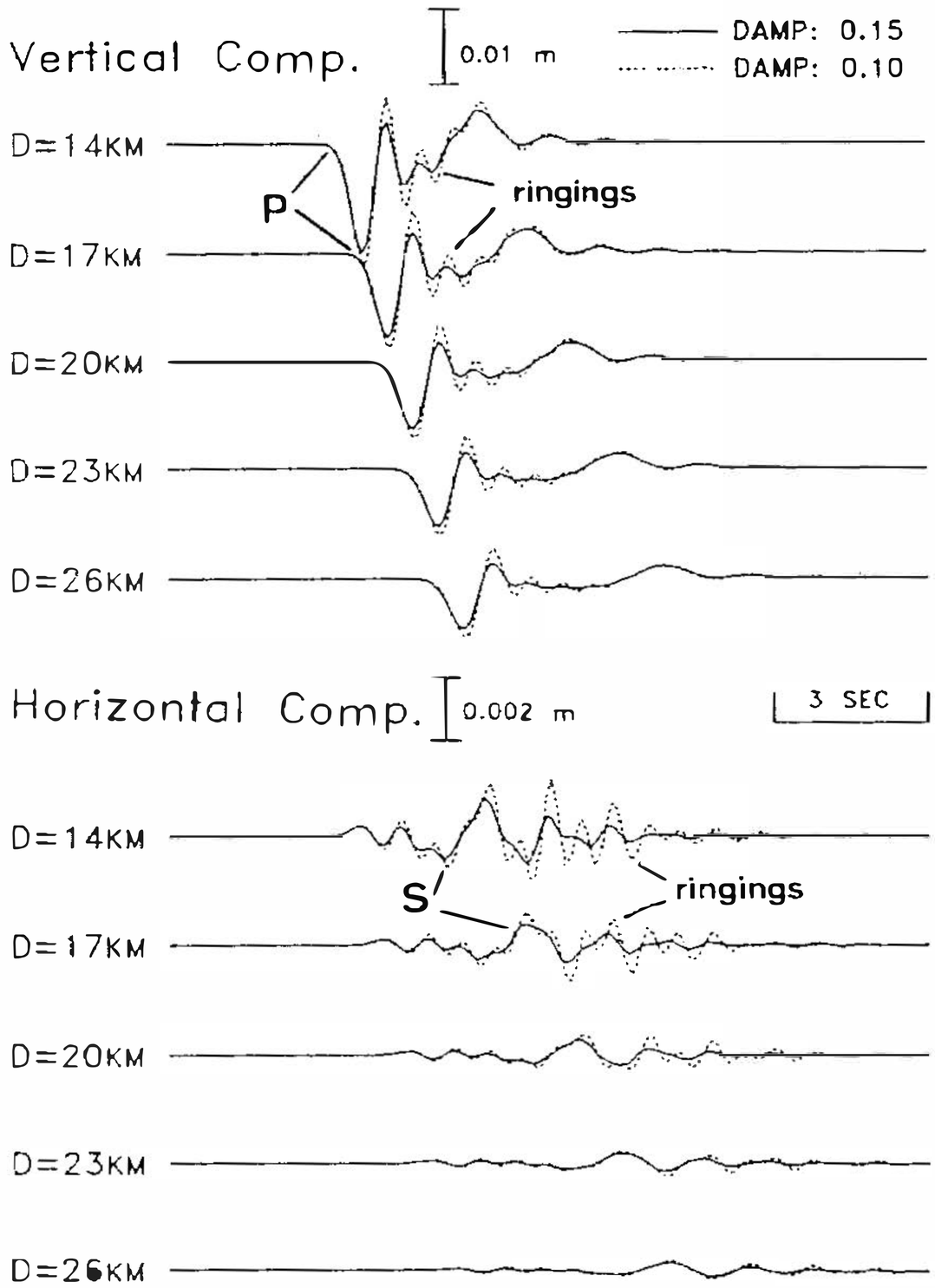

Fig. 2. Comparisons of the synthetic seismograms simulated by finite element modeling with a damping coefficient of 0.15 (solid lines) and 0.10 (dashed lines) at various distances. The amplitudes are exaggerated in the horizontal component. D represents distance.

A quantitative analysis of the reduction of the real signals due to the damping effect is necessary. The peak amplitude of first P motion is measured from the synthetic seismograms at each node along lines AA′ or BB′. Five decay patterns corresponding to different damping coefficients are shown in Figure 3(a). Beyond a distance of 10 km, a curve with a damping coefficient of 0.1 decays in the form of approximately $x^{-1.2}$, where x is the distance the wave propagates. Another curve obtained from a damping coefficient of 0.175 attenuates very closely to the form of $x^{-1.3}$. All these decay forms are determined by fitting with a group of standard exponential curves. In general, there is a linear relationship among these curves. The basic assumption here is that the factor caused by the damping involved in the numerical mesh relates to the exponential form of distance. The decay curves for the S-wave cases are also illustrated in Figure 3(b). Results show that a curve with a damping coefficient of 0.125 matches the form of $x^{-1.2}$. Moreover, the curve with a damping coefficient of 0.2 is the approximate form of $x^{-1.3}$. Therefore, it is obvious that S-waves are more weakly attenuated than relatively higher frequency P-waves because of the mentioned frequency-dependent specialty.

Finally, to elicit the damping effects of the amplitude, the geometrical spreading factor, which has the theoretical decay form of x^{-1} on the amplitude of the body waves, must be removed from the synthetic amplitudes. By simple algebraic calculations, the additional

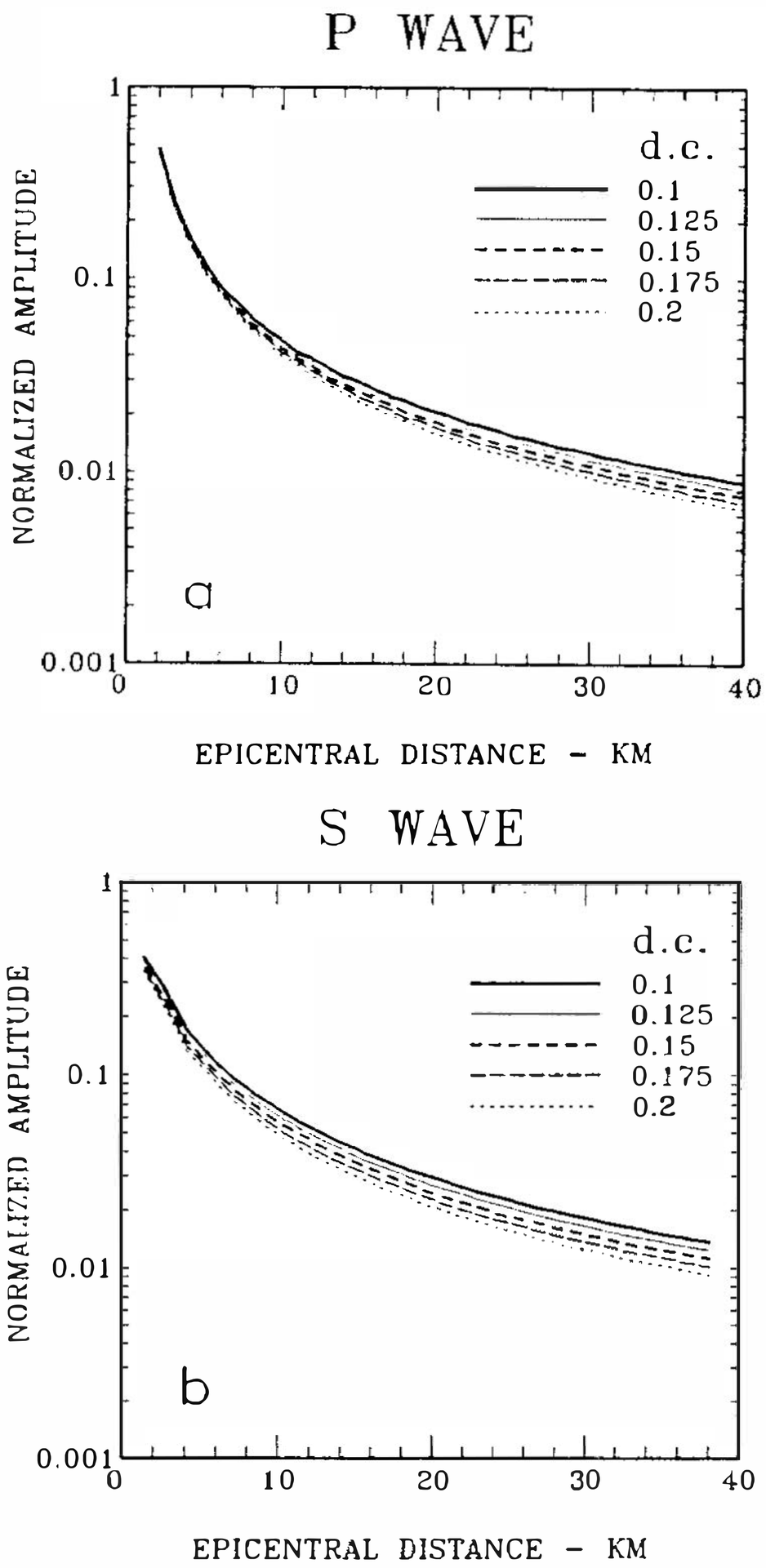

Fig. 3. The attenuation curves of (a) P-wave and (b) S-wave amplitude for various damping coefficients (abbreviated as d.c. in diagram).

suppression of amplitude due to the damping effect results in a factor of $x^{-0.07}$ approximately for the damping coefficient increment of 0.05 and the distance x in the period range in this study. This, in practice, perhaps is the best way that the amplitudes of seismograms synthesized by the finite element method can be corrected. The authors also analyzed the damping effect in the frequency domain and concluded the proper coefficient is 0.15 which coincides with that value suggested by Archuleta and Frazier (1978). Therefore, the following amplitude analyses are corrected using the method discussed above.

3. RESULTS AND DISCUSSIONS

Two simplified crustal models, one of the half-space and the other, a layer over half-space, are considered here. In the part of the half-space for both models, the P-wave velocity of the medium is 6.0 km/sec, while the S-wave velocity is 3.4 km/sec. The density is 2.6

gm/cm^3. For the top 3-km thick layer, the P and S-wave velocities are 3.4 km/sec and 1.7 km/sec respectively. The density of the layer is 1.8 gm/cm^3. These are the simplest models in which the Rayleigh waves can exist and propagate definitively.

As with the computations made by Yeh and Chung(1993), in addition to the point dislocation sources, finite faults with a length of about 3 km and dip angles of 26°, 45° and 63° are simulated, respectively. Only normal-faultings are discussed in this study. For the finite faults, the downgoing rupture unilaterally propagates from the upper point of the fault with the rupture velocity of 0.9β, where β is the shear-wave velocity. The slip is 1 m for the finite fault. In order to compare the amplitudes of the excited Rayleigh waves based on the same seismic moment of source, the slip for the point source is 3 m.

With the complex polarization analysis proposed by Vidale (1986), a typical pattern of Rayleigh wave particle motion polarized in the vertical direction can be clearly observed on the free surface for a certain source beyond the critical epicentral distance, as suggested by Yeh and Chung (1993). In their paper, they completely identified the wave type of a certain wavelet traced from source to the point where it converts to a Rayleigh wave, using not only the seismograms on the free surface but also those of the depth cross-section in order to check the eigenfunctions of the designed model and then derive the definite critical distance based on the ellipticity variation of particle motions. Detailed procedures are described in their paper. The ellipticities of the particle motion for typical Rayleigh waves were estimated to be in the range of 0.6 to 0.7 in the half-space model. Additionally, one important result shows that the critical epicentral distance is around 3 to 5 times the source depth for the point dislocation source in the half-space model. However, about 10 km of the critical distance was ambiguously obtained for both the point and finite sources in the one-layer over half-space model. When doing the complex polarization analysis in this study, the critical distances are recalculated using a longer time window and therefore involve the whole Rayleigh wavelet. These results allow for the amplitude variations of the Rayleigh waves at the critical epicentral distances to be further analyzed in this study. The purpose of this study, then, is to identify the maximum amplitude of a Rayleigh wave that can be generated and positively recognized in some epicentral distance by various source parameters (i.e., source depth, source dimension, and dip angle of the fault plane). Since the displacement waveforms in the near-source field are strongly controlled by the rupture mechanism, the peak-to-trough amplitudes in about one and a half cycles are analyzed to avoid bias in the measurements which may caused by the side-leaning of the waveforms. The amplitudes expressed in all cases of this paper are measured in the vertical component.

3.1. Comparisons for Various Structures

Figure 4(a) shows the comparison of Rayleigh wave amplitudes synthesized on the free surface of the half-space model and the one layer over half-space model respectively, for a 45° dip-slip point dislocation source located at different depths. Basically, the distances where the Rayleigh waves can be identified in the layered half-space model are shorter than those in the half-space model with source at the same depth (depicted with solid and open symbols with the same shape in the diagrams). Larger amplitudes are observed in the case of the layered half-space model for the shallower sources. It might be expected that more seismic energy trapped in the surface layer convert to surface waves. The reverse results are calculated for the deep sources. They can be explained by their eigenfunction characteristics in both structures. In addition, the waveforms become complicated and elongated by the low-velocity top layer (Figures 5(a) and 5(e)).

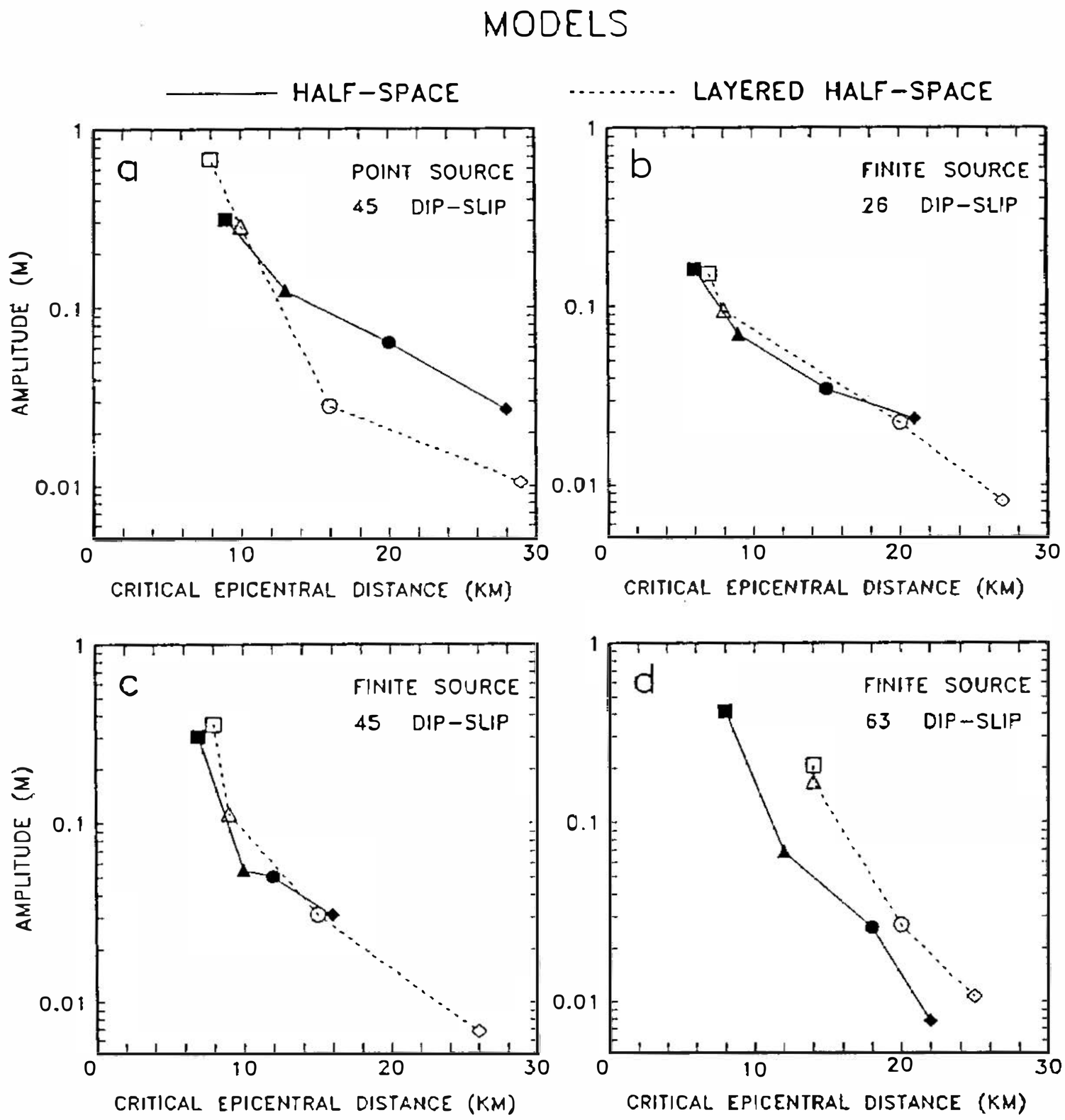

Fig. 4. The peak-to-trough amplitude variation of the traced waves measured on the free surface of the half-space model (solid lines) and of a layer over half-space model (dashed lines) for (a) 45° dip-slip point sources, and (b) 26°, (c) 45°, (d) 63° dip-slip 3 km long finite sources, respectively. The symbols of square, triangle, circle, and rhombus correspond to the source depths of 2 km, 4 km, 7 km, and 10 km, respectively. The epicentral distance represents the distance where the Rayleigh wave can be identified initially.

For the finite source of 3 km in length, the central point of the fault is taken to measure the depth universally. Figure 4(b) shows the results with a dip angle of 26°. Again, the Rayleigh wave amplitudes are generally stronger in the layered half-space model for only the shallower sources. The amplitude differences for shallower sources, however, are not as large as those for point sources. From the waveforms shown in Figures 5(b) and 5(f), the number of higher frequency signals observed is greater, while the typical particle motions of the fundamental mode Rayleigh waves are not even seen for the 2-km deep source in either model. Even though it is hard to distinguish clear Rayleigh waves in the waveforms, the complex polarization analysis does determine the critical distances by judging from ellipticity variations over the depth cross-section. It can easily be understood that the observations on the free surface are greatly affected by the rupture process along a shallower and closer horizontal-lying fault plane. Another phenomenon is that the selected Rayleigh waves dominate for a

relatively longer period in the cases of deeper sources than in those of the shallower ones. This can be explained by the characteristics of the eigenvector for the longer-period surface waves.

When the dip angle of the finite fault changes to 45°, the observed amplitudes (shown in Figure 4(c)) are still larger on the free surface of the layered half-space model, much like the situation in the previous cases. In this case, the source depth dependence of Rayleigh wave excitation is very clear. This characteristic can be found in the waveforms displayed in Figures 5(c) and 5(g). Obvious Rayleigh waves are generated by a 2 km deep source in a short distance for both models.

In the case of the steepest dip angle, some significant differences in the pattern of the relationship between the amplitude and critical epicentral distance are observed (Figure 4(d)). Although the distances required to generate well-defined Rayleigh waves in the layered half-space model are longer than those needed in the half-space model, the amplitudes for source depths of 4 km, 7 km and 10 km in the layered half-space model are still stronger than the others corresponding to the same depth in the half-space model. One of the possible reasons for this is that the dislocation of the ruptures along the steeper fault plane should have larger component in the vertical direction and provide more efficient mechanism to trap the energy within the top layer. Figures 5(d) and 5(h) show the displacement waveforms for such a case.

In general, stronger Rayleigh waves are excited in the layered half-space model than in the half-space model for the shallower sources. Simple and distinct waveforms are developed in the simple structure.

3.2 Comparisons for Various Source Length

In order to understand the effect of the source length on Rayleigh wave excitation, the results produced by a point source with a dip angle of 45° and a 3 km long finite source with the same dip angle are compared. At first, it is noted that, for a reasonable comparison, the slip of the point dislocation source is three times that of the finite fault because, on average, the rupture of the finite fault is distributed on three sequential split nodes.

Figure 6(a) shows the comparison for the half-space model. The Rayleigh wave amplitudes excited by a point source are evidently larger than those by a finite source although a longer distance is needed to develop well-identified surface waves. This phenomenon also exists in the layer half-space model (Figure 6(b)). When the amplitude ratios for the two various source lengths are examined visually, the amplitudes due to a point source are generally about 2-3 times those of a finite source at the same epicentral distance and source depth, which suggests the stronger Rayleigh waves are generated by the rupture type of energy released in high concentrations in time and space.

3.3 Comparisons for Various Dip Angles

For the half-space model, the Rayleigh wave amplitudes produced by finite sources with various dip angles are represented in Figure 7(a). A discrepancy in amplitude intensity appears with 2 km deep sources, which shows that stronger Rayleigh waves can be generated by a steeper dip-slip fault. However, for deeper sources, the amplitudes tend to have consistent levels when the dip angles are small. In addition, it should also be noticed that the Rayleigh waves observed at short distances for deeper sources with various dip angles do not exhibit complete waveforms (shown in Figures 5(b), 5(c) and 5(d)) although they can be recognized using polarization analysis. The comparisons for the layered half-space model are shown in

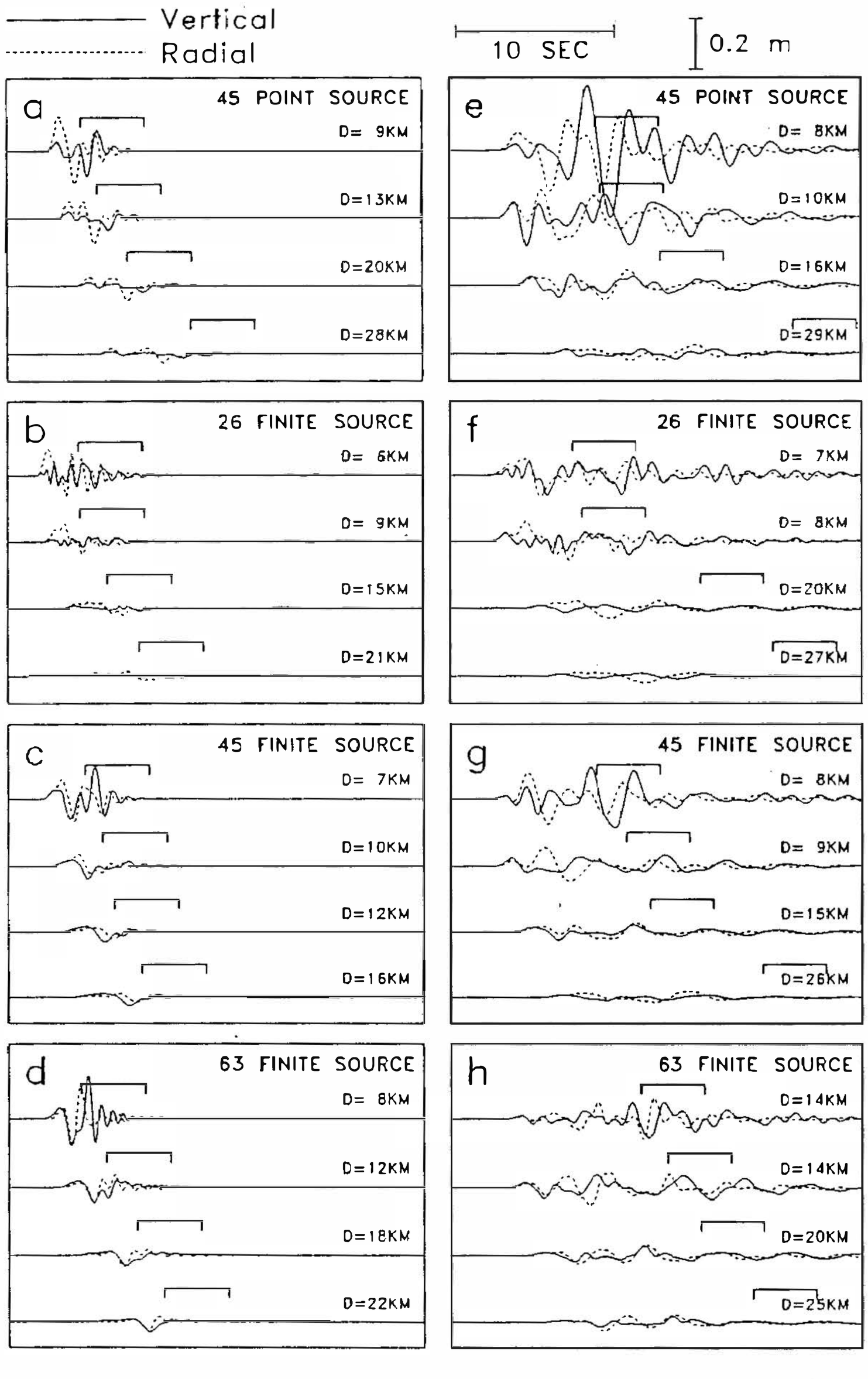

Fig. 5. The synthetic waveforms for various source mechanisms, explained at top right of each panel, for the half-space model ((a), (b), (c), and (d)) and for the layered half-space model ((e), (f), (g), and (h)), respectively. The epicentral distance is shown at the end of each trace. In each panel, four trace pairs from top to bottom are calculated by the source depth of 2 km, 4 km, 7 km, and 10 km, respectively. The identified Rayleigh waves are also marked by the time windows.

Figure 7(b). The results are basically similar to those of the cases in the half-space model except that with the 63° dip-slip finite sources, they strongly depend on the source depth.

On the basis of the above comparisons, it can be said the effect of source depth on surface wave excitation is significant. However, on the basis of waveform inspection, the well-defined Rayleigh waves should develop at longer distances than the results from Yeh and Chung (1993) for deeper sources indicate. Nevertheless, they can be recognized according to the ellipticity variations of the particle motions. Even if this point is considered, the relationships of the amplitude and the source parameters discussed in this study still do not generally change.

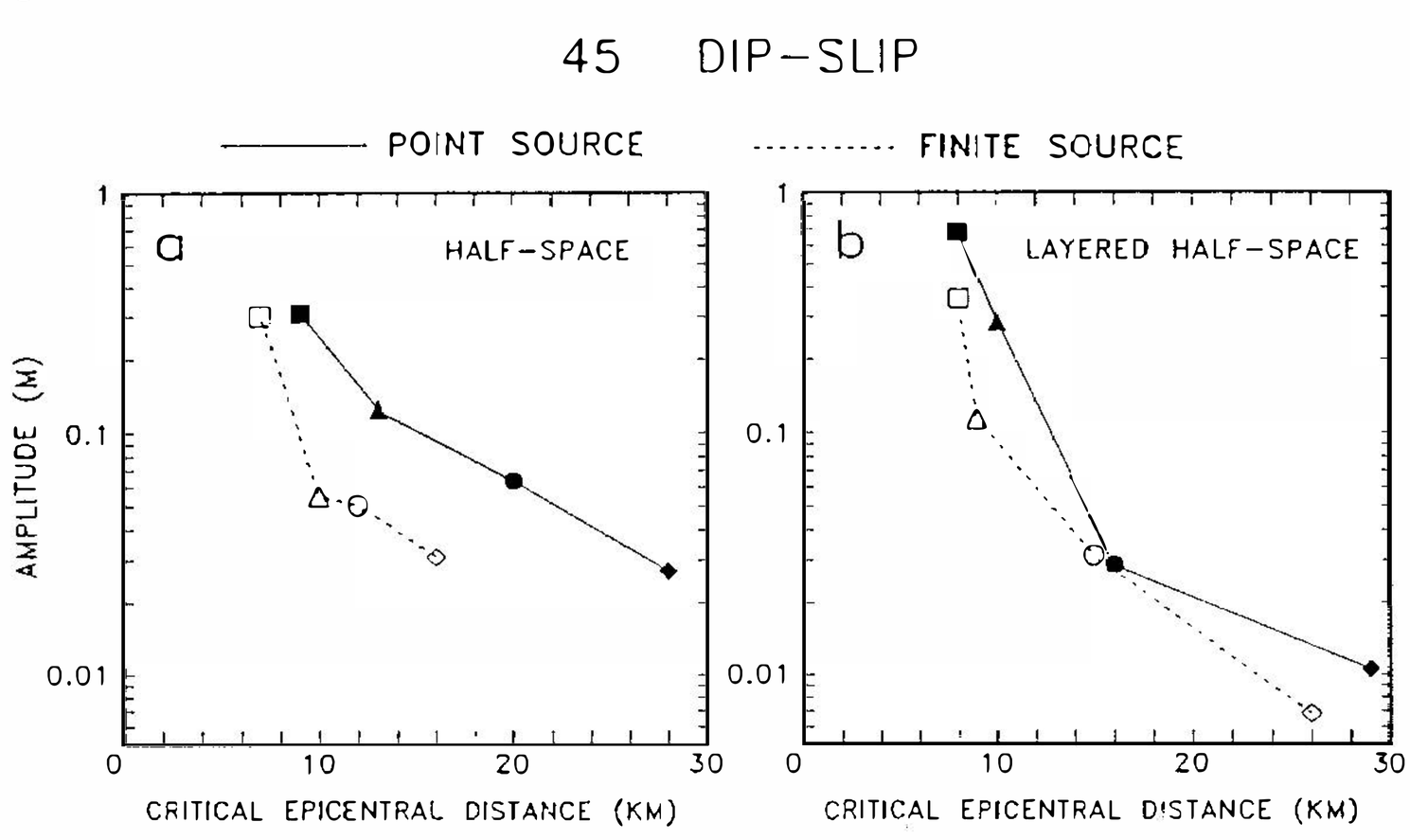

Fig. 6. The peak-to-trough amplitude variation for the point sources (solid lines) and the finite sources (dashed lines) with 45° dip-slip in the (a) half-space model, and (b) layered half-space model. Other explanations are the same as in the Fig 4.

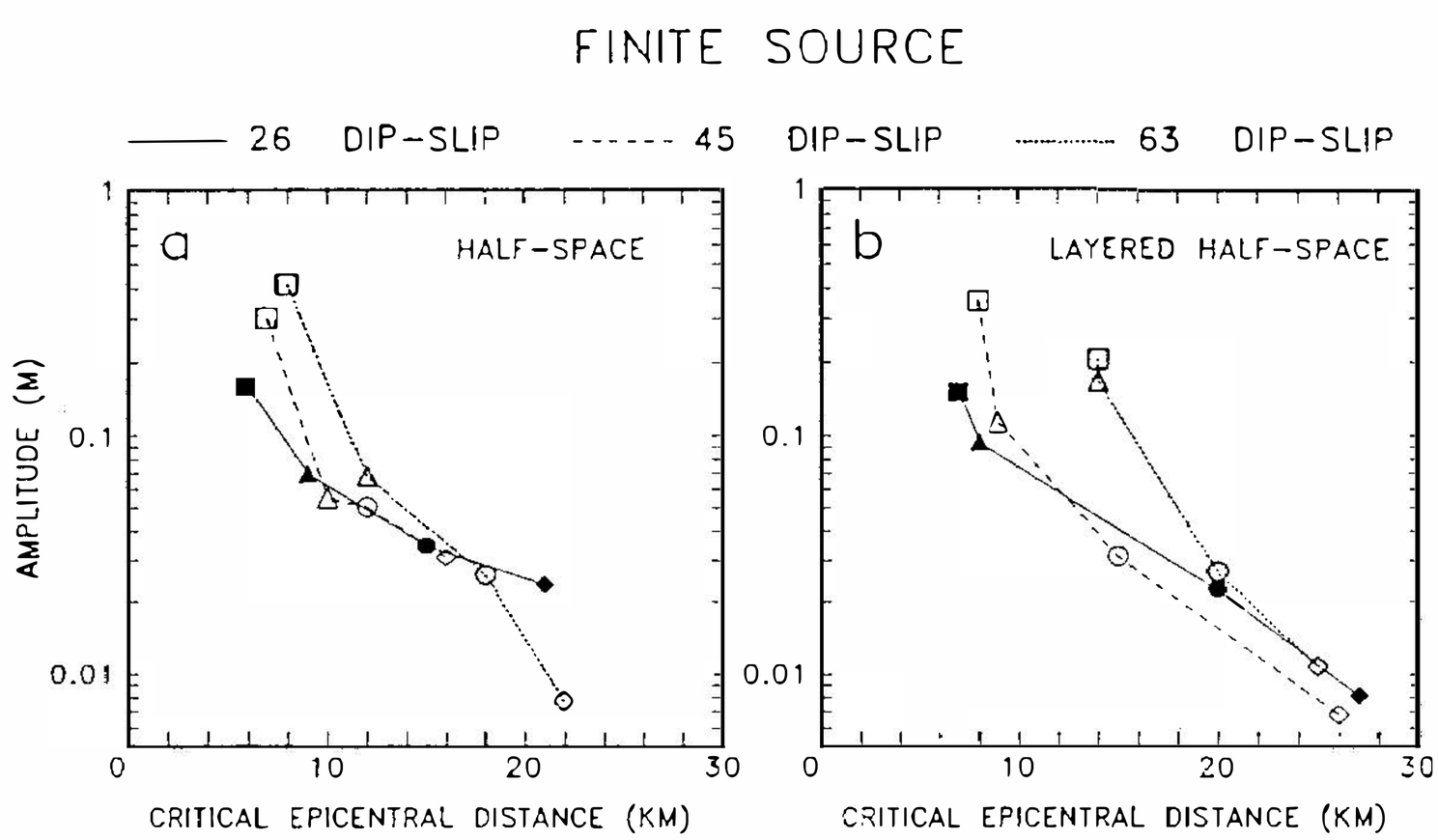

Fig. 7. The peak-to-trough amplitude variation for the 3 km long finite sources with 26° (solid lines), 45° (dashed lines), and 63° (dot lines) dip-slip rupture in the (a) half-space model, and (b) layered half-space model. Other explanations are the same as in the Fig. 4.

4. CONCLUSIONS

The amplitude variations of the short-period Rayleigh waves generated in the vicinity of the source are calculated using the two-dimensional finite element method. The numerical calculations involve the anelastic-like effect due to the damping factor to suppress the ringing phenomenon. Therefore, a simple method, as set out in previous paragraphs, is used to correct the calculated amplitudes to simulate the elastic medium.

A common characteristic is that Rayleigh-wave excitation from any type of source decreases with focal depth not only for the half-space model but also for the layered half-space model. In fact, this is easy to comprehend from the eigenvectors with respect to the source depth of theoretical surface waves. In general, stronger Rayleigh waves are excited in the layered half-space model than in the half- space model for the shallower sources. Additionally, stronger Rayleigh waves can be generated by steeper dip-slip faultings. Considering 45° dip-slip sources, it is also easier to generate stronger Rayleigh waves for point sources rather than finite sources.

From the results, it is clear that an earthquake source generates a short-period Rayleigh-wave response with complicated dependencies on both the source mechanism and the focal depth. At present, the modeling on the complex source is mature using the finite element technique. It provides an opportunity to understand the generation problem of the surface waves in the relative near-source region. As with previous long-period studies (e.g., Tsai and Aki (1971)), this investigation should offer a powerful method by which source parameters may be determined in the future.

Acknowledgments We are grateful to two anonymous reviewers for providing valuable comments. This work was supported by the National Sciences Council under grant NSC84-2111-M-001-001.

REFERENCES

Aki, K., and P. G. Richards, 1980: Quantitative seismology: Theory and Methods. Freeman, San Francisco, California, 932pp.

Archuleta, R. J., and G. A. Frazier, 1978: Three-dimensional numerical simulations of dynamic faulting in a half-space. *Bull. Seism. Soc. Am.*, **68**, 541- 572.

Gariel, J., R. J. Archuleta, and M. Bouchon, 1990: Rupture process of an earthquake with kilometric size fault inferred from the modeling of near-source records. *Bull. Seism. Soc. Am.*, **80**, 870-888.

Hanks, T. C., 1975: Strong ground motion of the San Fernando, California, earthquake: Ground displacements. *Bull. Seism, Soc. Am.*, **65**, 193-225.

Huang, B.-S., and Y. T. Yeh, 1991: Finite element reverse time imaging for earthquake sources and scatterers. *TAO*, **2**, 17-33.

Melosh, H. J., and A. Raefsky, 1981: A simple and efficient method of introducing faults into finite element calculations. *Bull. Seism. Soc. Am.*, **71**, 1391-1400.

Mendez, A. J., and J. G. Anderson, 1991: The temporal and spatial evolution of the 19 September 1985 Michoacan earthquake as inferred from near-source ground-motion records. *Bull. Seism. Soc. Am.*, **81**, 844-861.

Panza, G. F., F. A. Schwab, and L. Knopoff, 1972: Channel and crustal Rayleigh waves. *Geophys. J. R. Astr. Soc.*, **30**, 273-280.

Panza, G. F., F. A. Schwab, and L. Knopoff, 1973: Multimode surface waves for selected focal mechanisms. I. Dip-slip sources on a vertical fault plane. *Geophys. J. R. Astr. Soc.*, **34**, 265-278.

Shipley, S. A., H. G. Leistner, and R. E. Jones, 1967: Elastic wave propagation: a comparison between finite element predictions and exact solutions. Proc. Int'l Symposium on Wave Propagation and Dynamic Properties of Earth Materials, University of New Mexico Press, Albuquerque, 509-519.

Smith, W. D., 1974: A nonreflecting plane boundary for wave propagation problems. *J. Comp. Phys.*, **15**, 492-503.

Smith, W. D., 1975: A finite element study of the effects of structural irregularities on body wave propagation. PH. D. Dissertation, University of California, Berkeley.

Tsai, Y. B., and K. Aki, 1971: Amplitude spectra of surface waves from small earthquakes and underground nuclear explosions. *J. Geophy. Res.*, **76**, 3440-3452.

Vidale, J. E., 1986: Complex polarization analysis of particle motion. *Bull. Seism. Soc. Am.*, **76**, 1393-1405.

Yeh, Y. T., and J.-K. Chung, 1993: The effects of source on the generation of short period surface waves. *TAO*, **4**, 351-366.